Magneto-elastic effects in compressed cobalt from first-principles

Gerd Steinle-Neumann*
Bayerisches Geoinstitut, Universität Bayreuth, D-95440 Bayreuth, Germany
(Received 11 October 2007; revised manuscript received 4 February 2008; published 12 March 2008)

The magnetic structure and elastic constants of the close-packed phases of cobalt are computed as a function of compression using the linearized augmented plane-wave method with the generalized gradient approximation. The high-pressure phase transition from the hexagonal close-packed phase to the face centered cubic phase is correctly reproduced and is predicted to occur from a magnetic hcp to a nonmagnetic fcc phase, with a considerable change in aggregate elastic properties. At pressures well below the transition, an elastic anomaly is predicted in the hcp phase associated with the loss of magnetism under compression, which is most pronounced in the shear elastic constants. The magnetic nature of this anomaly provides an explanation for similar observations in experiments.

DOI: 10.1103/PhysRevB.77.104109 PACS number(s): 75.50.Cc, 71.15.Mb, 61.50.Ks, 75.30.Kz

I. INTRODUCTION

Characterizing the elasticity of transition metals under compression has been at the center of experimental development in high-pressure physics and geophysics over the past decade as the cores of the terrestrial planets are primarily composed of iron,[1,2] and an understanding of the high-pressure elasticity of iron would significantly advance the study of the internal structure of the Earth and other planets. As the study of elasticity on the high-pressure hexagonal close-packed (hcp) phase of iron has proven challenging, a lot of effort has focused on the metal adjacent to iron in the Periodic Table: cobalt. The study of cobalt provides a number of advantages over iron as follows: (1) cobalt crystallizes in the hcp phase at ambient conditions, while the hexagonal phase of iron cannot be quenched to low pressure; (2) it is possible to study single crystal elastic properties of cobalt, while, to date, no single crystal of hcp iron has been grown, even at high pressure; (3) the ambient pressure stability of cobalt allows for a direct cross-check and refinement of newly developed techniques through a comparison with conventionally obtained elastic constants, e.g., ultrasonic measurements at room conditions. However, a major drawback in using cobalt as an analog material for hcp iron is the fact that cobalt is ferromagnetic, while hcp iron is thought to be nonmagnetic based on a number of experimental studies.[3–6] In order to properly interpret the experiments on elasticity in cobalt, its magnetic state must be well understood to be of any significance in predicting the high-pressure elasticity of iron.

The pressure-temperature (P-T) phase diagram of cobalt shows a number of interesting features.[7] As mentioned above, the ambient pressure phase is ferromagnetic hcp, often coexisting with the cubic close-packed [face centered cubic (fcc)] phase.[8] At a temperature near 700 K, cobalt transforms martensitically to the fcc phase[9,10] retaining a magnetic moment:[11] the Curie temperature of fcc cobalt is 1388 K.[11] Cobalt melts at 1768 K.[12] Under compression, hcp cobalt also undergoes a phase transition to the fcc phase in the range of 100–150 GPa, with a wide coexistence region of the hcp and fcc phases.[7] There is no apparent volume change across the phase transition, but compressibilities of the hcp phase below and the fcc phase above the transition appear to change. The difference in compressibility between the two phases was inferred to occur due to the magnetic collapse across this phase boundary.[7]

The magnetic nature of the high-pressure phase and the question of a closed phase boundary in P-T space between hcp and fcc have been the subject of debate.[7,13] Recent high-pressure experiments using x-ray magnetic dichroism[6] show a strong uniform decrease of magnetism with compression.[6] This magnetic behavior appears inconsistent with a slight increase in the Curie temperature with pressure up to at least 25 GPa (Refs. 14 and 15) and density functional theory (DFT) based computations.[15–17] They predict a slight decrease in magnetic moment with pressure, with a rapid loss of magnetic moment starting near 65 GPa in the hcp phase.[16,17] The hcp phase, however, retains a finite magnetic moment up to the phase transition to the fcc phase.[16,17] The fcc phase is predicted to be nonmagnetic in its stability field;[17] it is ferromagnetic at low compression, but loses its magnetic moment near 100 GPa.

In experiments, the high-pressure phase transition appears to be preceded by an anomalous elastic behavior in the hcp phase. Measurements of the Raman active transverse optic (TO) phonon mode, which can be related to the shear elastic constant c_{44},[18,19] show a change in slope near 60 GPa.[13] This behavior has been confirmed by phonon computation on hcp cobalt, where a similar change was predicted in the slope of the TO mode at pressures near 75 GPa.[17] The measurements of aggregate elastic constants by both impulsive stimulated light scattering[13] (ISLS) and inelastic x-ray scattering[20] (IXS) show an even more pronounced anomalous behavior, with the shear modulus softening in the range of $\sim$70–100 GPa. This is best seen in deviations from an expected linear density dependence of longitudinal (v_L) and transverse (v_T) acoustic velocities (Birch's law), with a sublinear relation and even softening in v_L and v_T. As this softening occurs well below the phase transition pressure, it has been attributed to magneto-elastic effects, which are supported by the onset of a loss of magnetic moment in hcp cobalt predicted by the DFT computations.[16,17] There have been additional studies on the high-pressure elasticity of hcp cobalt, with single crystal studies using IXS,[21] ISLS,[22] and

radial x-ray diffraction (XRD),[23] but these studies do not reach the critical pressure region above 60 GPa.

Here, we perform DFT based computations on the magneto-elastic properties of both close-packed phases of cobalt by expanding on previous computational work,[16,17] paying particular attention to the effect of magnetism on the elastic constants, and trying to elucidate the experimental findings. To this effect, we compare the results from ferromagnetic (spin polarized) computations to nonmagnetic results. We organize the paper as follows: after introducing the computational method, we show and discuss the results for the magnetic structure, phase transition, and equations of state of the close-packed phases of cobalt, the magnetic collapse under pressure, and the elasticity of the two phases. Conclusions are given in the final section.

II. COMPUTATIONS

We investigate the energetics of the close-packed phases of cobalt using the full-potential linearized augmented plane-wave method[24] (LAPW) with the generalized gradient approximation (GGA) to the exchange-correlation potential.[25] GGA has been shown repeatedly to accurately describe bonding in transition metals.[16,26,27] We perform computations for both ferromagnetic (spin polarized) and nonmagnetic systems, allowing for a direct assessment of the influence of spin on physical properties.

The choices made for the computational setup are consistent with earlier work:[16] core states (up to $3s$) are treated fully relativistically using the full Dirac equation. The valence states ($3p$, $3d$, $4s$, and $4p$) are treated in a semirelativistic approximation, neglecting spin-orbit coupling. We use a $16\times16\times16$ special k-point mesh[28] for both the fcc and hcp phases. $R_{MT}*K_{\max}=9.0$ determines the basis set. With these parameters, relative energies are converged to better than 0.1 mRy/atom and magnetic moments to better than $0.05\mu_B$.

Computations are carried out over a wide range of compression, between 50 and 75 Bohr^3, corresponding to $0.65V_0-1.0V_0$ (for the equation-of-state computations, volumes up to 85 Bohr^3 are used). For the hcp phase, we have optimized the ratio of the lattice constants (c/a) at each volume by performing calculations for several different values of c/a ($c/a=1.55$, 1.6, 1.65, and 1.7). The equation of state is obtained by describing the energy-volume curve with a third order expansion in finite Eulerian strain [Birch–Murnaghan equation of state (BM EOS)].[29] Unlike previous computational work,[17] we do not add zero point motion or thermal expansion to the EOS as this distorts the computational results: such additions will increase V_0 by 1%–2% and decrease K_0 by 5% for the close-packed phases of cobalt.

For the hcp phase, elastic constants are computed from the bulk modulus obtained from the equation of state, the relative compressibility of the hexagonal axes, and strain-energy relations using four strains for the hcp cell.[16] For the fcc phase, the bulk modulus and two strains are used.[30] We apply isochoric (volume conserving) strains (ε) to the cell, which is important for an accurate determination of elastic constants under compression.[31] Aggregate moduli and aggregate acoustic velocities are computed from single crystal elastic constants using Voigt and Reuss averaging.[32]

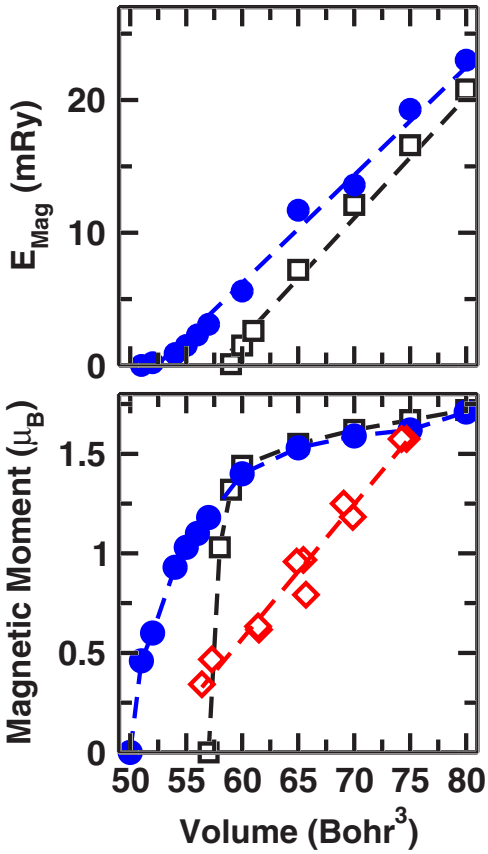

FIG. 1. (Color online) Magnetic moment (lower panel) and magnetization energy (upper panel) for the hcp (blue circles) and fcc phases (open squares). The magnetic moment data from x-ray dichroism (red open diamonds; Ref. 6) are given for comparison. Dashed lines are drawn to guide the eyes.

III. RESULTS AND DISCUSSION

A. Magnetism

We find a ferromagnetic phase with magnetic moments of 1.67 and $1.62\mu_B$ at 75 Bohr^3 for the hcp and fcc phases of cobalt, respectively (Fig. 1). The associated magnetization energies (relative to the nonmagnetic computation) are 19.3 and 16.6 mRy, respectively (Fig. 1). Under compression, the magnetization energy linearly decreases, with $\sim$0.81 mRy/Bohr^3 for the hcp phase and $\sim$0.91 mRy/Bohr^3 for the fcc phase (Fig. 1). The associated magnetic moments slowly decrease to a compression of up to 60 Bohr^3. At higher compression, the magnetic moment is almost instantaneously lost from the fcc phase; for the hcp phase, it more slowly vanishes, reaching zero at 50 Bohr^3 (Fig. 1). The loss of magnetism is consistent with previous computational results,[16,17] and a dense volume sampling in the loss region used here provides a detailed picture. As mentioned above, the initial slow decrease in magnetic moment is consistent with a slight increase in the Curie temperature of Co with pressure,[14,15] but is in conflict with x-ray magnetic circular dichroism results[6] where a uniform decrease in

magnetic moment with compression is reported (Fig. 1). A critical reassessment of high-pressure magnetism in cobalt, for example, by establishing an initial pressure slope of magnetic moment by neutron diffraction, is clearly advised.

B. Phase stability and equation of state

In agreement with experiments and previous computations, we find hcp cobalt stable over the fcc phase for a large volume range (Fig. 2), from overexpanded volumes (~85 Bohr^3) to ~55 Bohr^3. If one considers the energies obtained directly from the computations, the transition is located at a volume of 56 Bohr^3 or a pressure of ~105 GPa. If the fitted energies from the equations of state for the magnetic phases are used (Table I), the transition occurs at 52.5 Bohr^3 (~145 GPa), with both values within the coexistence region of the fcc and hcp phases in experiments.[7] This large variation stems from the fact that the magnetization energy mentioned above is nearly linear with volume (Fig. 1) and fitting the closed expression for the BM EOS yields a poor fit in the region of magnetic loss in both phases. Magnetism in the hcp phase just vanishes in the structural phase transition region.

Despite the difficulty in fitting, the EOS for magnetic hcp cobalt is in good agreement with the latest experiments[33] (Table I). At 55 Bohr^3 (~110 GPa), the pressures are within 3 GPa, while there are larger discrepancies with earlier experiments[7,8] and computations[17] (Table I, Fig. 2). However, all of these studies are within 20 GPa at 55 Bohr^3. The EOS of the fcc phase shows a considerable difference between various studies (Table I). By comparing the P-V EOS, it becomes apparent that for a good determination, the metastable low-pressure data, used by Fujihisa and Takemura,[8] are critical to determine a robust V_0 (Table I). Also, the computational equation of state using the plane-wave self-consistent field (PWSCF) method[17] shows a considerably softer behavior than the experimental data[7,8] or the LAPW results reported here: for a volume of 50 Bohr^3 (~175 GPa), the PWSCF results are at least 25 GPa lower than all the other equations of state.

The linearity of the magnetization energy (Fig. 1) suggests an alternative fitting scenario, combining a nonmagnetic equation of state with a magnetic pressure ($P_{mag} = -\partial E_{mag}/\partial V$) in the region of ferromagnetism. This yields a value of 12 GPa for hcp cobalt and 13 GPa for fcc cobalt. Adding this magnetization pressure to the nonmagnetic equation of state (Table I) would lead to a volume change of 1% at the magnetic transition pressure. Performing separate equation-of-state analyses for the nonmagnetic E-V curve and the magnetization energy also decreases the discrepancy in ΔE-V for the results of the computations and the fitted EOS (Fig. 2).

In order to understand the metastable presence of the fcc phase at low pressure[8] and the phase transformation mechanism both at high temperature and pressure,[7,10] as well as to characterize the small energy difference between the two close-packed phases, a characterization of the axial ratio (c/a) in the hcp phase is essential. In our computations, the axial ratio c/a is nearly constant (1.615) up to a compression

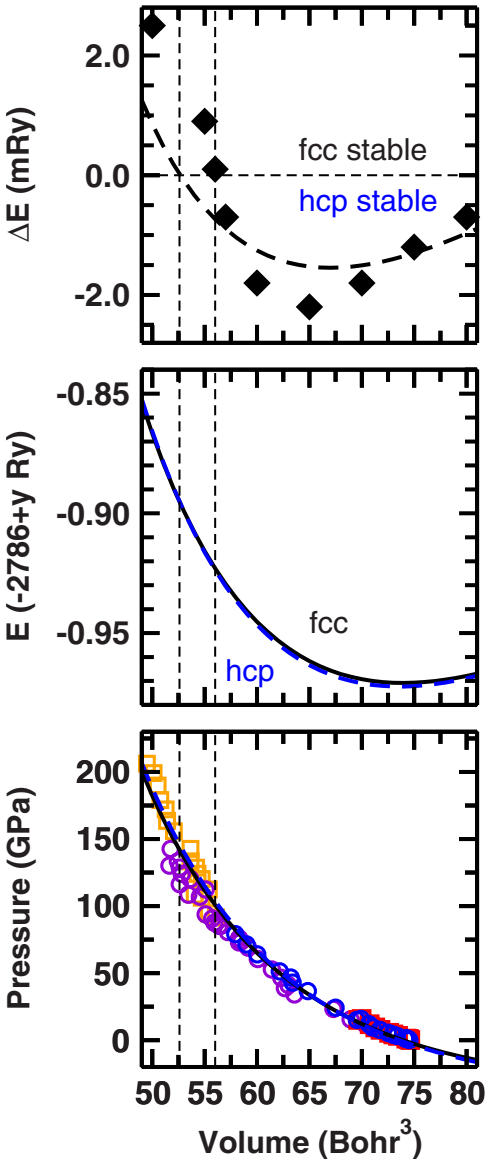

FIG. 2. (Color online) Energetics and equation of state for cobalt. In the upper panel, filled symbols show the energy difference at the volumes computed and the dashed line shows the energy difference from the fitted equations of state. The vertical fine dashed lines show the volume of phase transition from the computational results (right line) and after the equation-of-state fit (left line). E-V equation of state for the hcp (blue dashed) and fcc phases of cobalt are shown in the middle. The lower panel shows the resulting P-V equation of state for fcc (solid black line) and hcp cobalt (dashed blue line) in comparison to experimental data from Ref. 8 (hcp, blue circles; fcc, red squares) and Ref. 7 (hcp, violet circles; fcc, orange squares).

of 65 Bohr^3 (~40 GPa); at lower volumes, c/a increases up to 1.62 at 50 Bohr^3.

C. Elasticity

At ambient pressure (V=75 Bohr^3), the elastic constants for the magnetic hcp phase are in good agreement with ultrasonic experiments[34–36] (Fig. 3). For the longitudinal (c_{11}

TABLE I. Equation-of-state parameters for third order finite-strain fits for magnetic (fm) and nonmagnetic (nm) phases of hcp and fcc cobalt. Other abbreviations are explained in the text. Values with an asterisk (*) are fixed in the fit.

	Phase	Ref.	V_0 (Bohr^3)	K_0 (GPa)	K_0' (GPa)
hcp	LAPW GGA fm	This study	73.6	210	4.1
	LAPW GGA nm	This study	69.6	256	4.7
	LAPW GGA fm	16	73.6	212	4.2
	LAPW LDA fm	16	68.0	255	4.0
	LAPW GGA fm	17	74.0	205	
	PWSCF GGA fm	17	74.4	189	4.8
	Experiment	8	74.9	199	3.6(2)
	Experiment	7	74.3	199	3.6
	Experiment	33	74.7*	202	3.9
fcc	LAPW GGA fm	This study	73.9	198	4.3
	LAPW GGA nm	This study	69.4	258	4.7
	LAPW GGA fm	17	73.8	247	
	PWSCF GGA fm	17	74.0	214	3.2
	Experiment	8	74.8	180	4*
	Experiment	7	69.8	224	5.8

and c_{33}) and the off-diagonal (c_{12} and c_{13}) constants, only c_{11} shows a significant difference, with the LAPW results overestimating the modulus by ~20 GPa (~6%). For the shear elastic moduli (c_{44} and c_{66}), c_{66} agrees with experiments, while c_{44} is overestimated by ~20% (90 GPa, compared to 75 GPa from experiment). The computed c_{44} also disagrees with the previous computations on the transverse optical phonon mode (~140 cm^{-1}) (Ref. 17) that, when transformed to c_{44},[19] yield a value of 70 GPa. In order to assess this value, we have also computed the zone center phonon mode with the frozen phonon approximation at 75 Bohr^3 and also find a value of 140 cm^{-1}, which is inconsistent with the c_{44} computed from strain-energy density. This and a comparison of the experimentally determined phonon frequency of the transverse acoustic mode[9] (135 cm^{-1}, corresponding to c_{44}=67 GPa) with the ultrasonic measurements[34] show the limitations of the force model in relating the TO mode and the c_{44} shear elastic modulus.[18,19] The shear anisotropy ratio (c_{44}/c_{66}) found here ($c_{44}/c_{66}>1$) is in agreement with ultrasonic measurements[34] and IXS measurements at ambient conditions,[21] but the ISLS measurements at zero pressure[22] show $c_{44}<c_{66}$.

The nonmagnetic elastic constants allow for an assessment of the magneto-elastic effects in cobalt. At ambient pressure, the shear elastic moduli and c_{13} show the largest difference between magnetic and nonmagnetic moduli: magnetic constants for c_{44} and c_{13} are larger than their nonmagnetic counterparts, c_{66} is significantly smaller (Fig. 3).

Under initial compression, the computed elastic moduli stiffen, with a compression slope consistent with experimental estimates from IXS[21] and ISLS[22] (Fig. 3), except for c_{13} and c_{44}. For c_{44}, the slope from the computations is steeper than in experiments, reaching a value of 165 GPa at 65 Bohr^3 compared to ~125 GPa in the IXS experiments.[21] For c_{13} at pressure near 25 GPa (67 Bohr^3), the experimental slope[21] becomes significantly steeper. In contrast to ISLS studies,[13,22] Raman measurements[13] or computations,[17] and IXS,[21] the radial XRD measurements[23] yield shear elastic constants c_{44} that are too large by a factor of 2 even at low pressure, which is consistent with a previous comparison for hcp rhenium.[16,37] c_{44}/c_{66} remains positive for the LAPW results, agreeing with the ISLS measurements up to 10 GPa.[22] In contrast, the IXS measurements show $c_{66}>c_{44}$ above 10 GPa.[21]

Where absolute differences between nonmagnetic moduli and ferromagnetic constants exist, the pressure slopes are similar, and for the nonmagnetic moduli, the volume dependence can readily be fitted with an Eulerian-strainlike expression over the whole compression range considered (Fig. 3). In contrast, for the magnetic hcp phase, the elastic moduli for magnetic hcp cobalt start to deviate from a monotonic increase at volumes below 60 Bohr^3 (~65 GPa) (Fig. 3). The shear elastic constants show a significant softening to the extent that the value for c_{44} at 57.5 and 55 Bohr^3 is smaller than the one at 60 Bohr^3. Similarly, the value for c_{66} at 55 Bohr^3 is smaller than the one at 57.5 Bohr^3. This coincides with the onset of a loss of magnetism in the hcp phase (Fig. 1), and once the magnetism has been completely lost in hcp cobalt, the shear moduli coincide with their nonmagnetic counterpart (Fig. 3). This behavior should also be expected in the TO phonon mode, and a change in slope is indeed observed in the measurements.[13] The computations[17] show a change in slope near 75 GPa, but the magnetic computations continue to show a smaller wave number than for the nonmagnetic phase, up to pressures far exceeding the loss of magnetization.

Both longitudinal elastic constants also show a smaller rate of increase in the compression range between 60 and

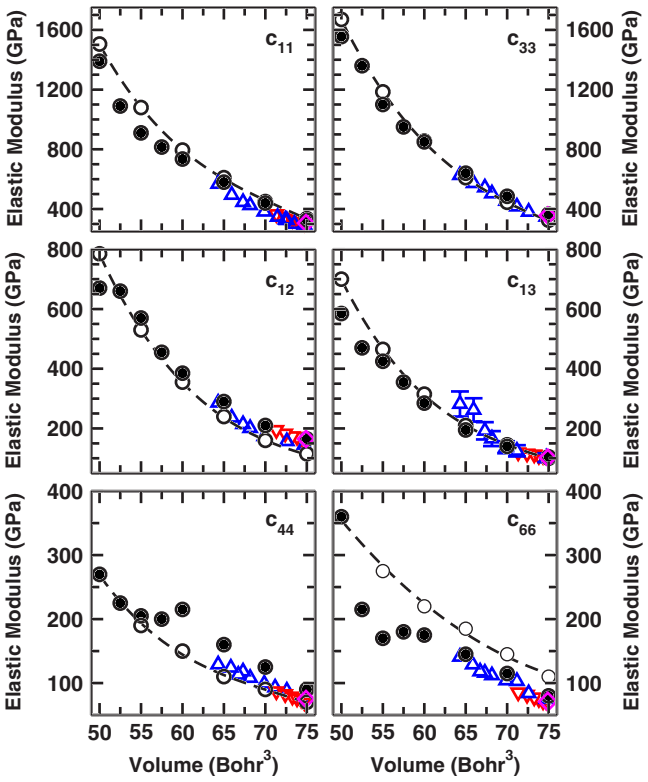

FIG. 3. (Color online) Single crystal elastic constants of hcp cobalt. Filled circles show the results from the magnetic computations and open circles from the nonmagnetic computations. The nonmagnetic results are fitted with a finite-strain expression (dashed lines). Experimental results for single crystal elasticity are included for ultrasonic measurements at ambient pressure (purple diamonds; Ref. 34), inelastic x-ray scattering (blue up triangles; Ref. 21), and impulsive stimulated light scattering (red down triangles; Ref. 22). Experimental error bars are included for c_{13}; for the other moduli, the error estimates are within the symbol's size.

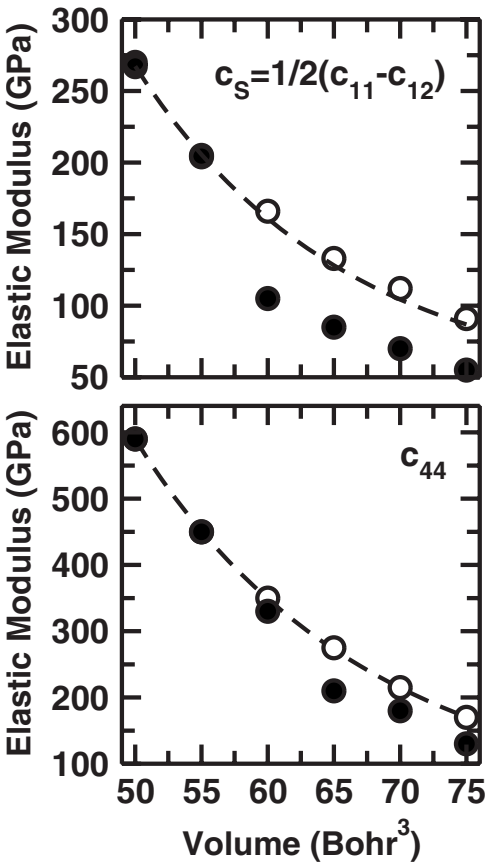

FIG. 4. Elastic moduli for fcc cobalt as a function of compression. Nonmagnetic (open circles) and magnetic (filled circles) values for c_{44} (bottom) and $c_s=1/2(c_{11}-c_{12})$ are shown. Nonmagnetic values are fitted with a finite-strain expression (dashed lines).

50 Bohr^3; this is much stronger in c_{11}, and for both moduli, there is still a difference between the magnetic and nonmagnetic phases at 50 Bohr^3 that can be traced back to the difference in bulk modulus between the magnetic and nonmagnetic phases. For the off-diagonal constants, the pressure dependence between magnetic and nonmagnetic phases is consistent with a deviation only at the smallest volumes. As in the case of the longitudinal moduli, this can be traced to the difference in bulk modulus.

The strong magneto-elastic coupling in the shear elastic constants computed here for hcp cobalt at high pressure, the TO phonon mode measured[13] and computed,[17] as well as the anomaly in v_T and v_L measured by ISLS[13] and IXS[20] show that cobalt can be used as an analog to hcp iron, but only with great caution.

In fcc cobalt, there is also a considerable difference between the magnetic and nonmagnetic elastic constants. Rather than through the single crystal elastic constants (c_{11}, c_{12}, and c_{44}), this difference is shown through c_{44} and $c_s=1/2(c_{11}-c_{12})$, which are computed directly by the strain-energy density[30] (Fig. 4). For both of these moduli, the magnetic constants have a lower value than the nonmagnetic constants. At volumes below the magnetic transition (55 Bohr^3), the elastic constants merge with the nonmagnetic values, and there is only a slight softening of c_{44} near the transition (65 Bohr^3). As in the case of hcp cobalt, the nonmagnetic elastic moduli can readily be fitted with an Eulerian finite-strain expression (Fig. 4).

The aggregate acoustic velocities reflect the anomalies in the single crystal elastic constants (Fig. 5). For the magnetic and nonmagnetic hcp phases, v_T and v_L are similar at low compression and linearly depend on density, following Birch's law[38] (Fig. 5). For the nonmagnetic velocities, this dependence continues for the whole compression range, while v_T for the magnetic phase shows a strong softening, which decreases over some compression range before recovering the nonmagnetic value at highest density. The v_L for magnetic hcp shows a slight deviation from the linear dependence. The compression dependence of aggregate velocities agrees well with experiments to above 100 GPa,[13,20] except for v_L at highest pressure, where the ISLS experiments[13] show a stronger softening (Fig. 6). The good agreement between the measurements and the computations for magnetic hcp cobalt also indicate that cobalt remained in the hcp structure to the highest pressure in all experiments.[13,20]

fcc cobalt shows large differences in elasticity between magnetic and nonmagnetic structures: at low compression, the magnetic velocities for the fcc phase are close to the values for the hcp phase, while the nonmagnetic velocities

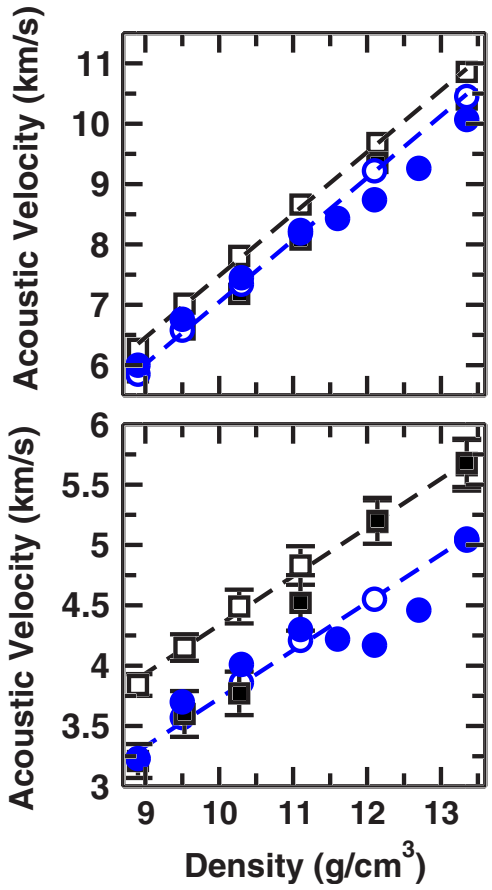

FIG. 5. (Color online) Transverse (bottom) and longitudinal (top) aggregate acoustic velocities for magnetic (filled blue circles) and nonmagnetic (open blue circles) hcp cobalt as a function of density. Aggregate velocities for fcc cobalt are shown with squares; open symbols are for the nonmagnetic computations and filled squares for magnetic fcc cobalt. Dashed lines are linear fits of nonmagnetic fcc (black) and hcp (blue) velocities. Bars show the variation between Voigt and Reuss averages for v_T and v_L. Where no bars are shown, the variations are within the symbol's size.

are considerably larger. Magnetism is lost from the fcc phase at lower compression (Fig. 1) and the acoustic velocities for the magnetic phase change smoothly to the values of the nonmagnetic phase (Fig. 5). Again, acoustic velocities for nonmagnetic fcc cobalt follow Birch's law over the whole compression range (Fig. 5).

Across the phase transition between the hcp and fcc phases, considerable changes in the aggregate velocities are predicted: for v_T, we predict an increase of more than 10%; for v_L, an increase in the range of 5%–10% can be expected, depending on the exact location of the phase transition (Fig. 5). Such a change has not been observed to date in experiments as the relevant pressure range has not yet been reached for the measurements of elastic properties.

As we have shown above, the phase transition is preceded by the loss of magnetism in hcp cobalt and the associated elastic softening, in particular, for the hcp phase. This indicates that the phase transition is quite different from the hcp-fcc transition at high temperature, where only the c_{44} elastic constants show a continuous decrease (by ~25%) just below the phase transition temperature.[9,36,39]

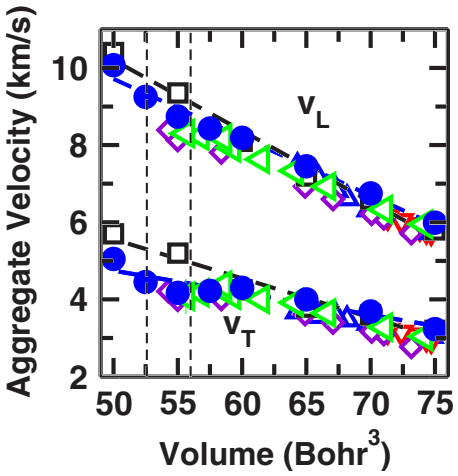

FIG. 6. (Color online) Aggregate acoustic velocities for cobalt. The results for the hcp (blue circles) and fcc phases (black open squares) are compared with experimental data from inelastic x-ray scattering (blue up triangles, Ref. 21; green triangles left, Ref. 20) and impulsive stimulated light scattering (red down triangles, Ref. 22 purple diamonds, Ref. 13).

IV. CONCLUSION

As a function of compression, we computed the magnetic structure, equation of state, and elastic constant tensor for the close-packed phases of cobalt to study the magneto-elastic effect under pressure and the nature of the phase transition from the hcp to fcc phase above 100 GPa. The results presented here provide a critical framework for the understanding and interpretation of high-pressure experiments on the elasticity of cobalt and the nature of the hcp-fcc phase transition. We find that in both phases, the magnetic moment is lost, starting at 60 Bohr^3. In the fcc phase, the magnetism is almost instantaneously squeezed out; in the hcp phase, it is lost over a range of ~10 Bohr^3. The phase transition occurs from the magnetic hcp phase to the nonmagnetic fcc phase in the range of 52.5–56 Bohr^3 (105–145 GPa), which is in excellent agreement with experiments.[7] In the loss region of magnetism, there is a considerable elastic anomaly in hcp cobalt, which shows a significant softening of the shear elastic constants c_{44} and c_{66} and is also reflected in v_T. There is a less pronounced anomaly in the longitudinal moduli and v_L. This magnetically induced elastic anomaly provides an explanation for the anomalies in acoustic velocity observed in ISLS and IXS experiments.[13,20] The strong magneto-elastic coupling for hcp cobalt shows that this metal can be used as an analog for hcp iron at high pressure with great caution.

In contrast to the hcp phase, there is no anomaly in the elasticity of fcc cobalt under compression; at the loss of magnetism, the elastic constants of the magnetic phase merge gradually with those of the nonmagnetic phase. Across the phase transition from hcp to fcc cobalt, an increase in both acoustic velocities is predicted: more than 10% for v_T and at least 5% for v_L. Such an increase has not yet been observed in experiments on the elasticity of cobalt, as the relevant pressure range has not yet been reached.

ACKNOWLEDGMENTS

I thank H. Krakauer and D. Singh for the use of their LAPW code, and greatly appreciate helpful discussions with D. Antonangeli, R. E. Cohen, A. Goncharov, R. J. Hemley, and L. Stixrude. Comments by D. Antonangeli and K. K. M. Lee significantly improved the manuscript.

*g.steinle-neumann@uni-bayreuth.de

[1] F. Birch, J. Geophys. Res. **57**, 227 (1952).
[2] A. Jephcoat and P. Olson, Nature (London) **325**, 332 (1987).
[3] J. P. Rueff, M. Krisch, Y. Q. Cai, A. Kaprolat, M. Hanfland, M. Lorenzen, C. Masciovecchio, R. Verbeni, and F. Sette, Phys. Rev. B **60**, 14510 (1999).
[4] S. Nasu, T. Sasaki, T. Kawakami, T. Tsutsui, and S. Endo, J. Phys.: Condens. Matter **14**, 11167 (2002).
[5] O. Mathon, F. Baudelet, J. P. Itie, A. Polian, M. d'Astuto, J. C. Chervin, and S. Pascarelli, Phys. Rev. Lett. **93**, 255503 (2004).
[6] V. Iota, J. H. P. Klepeis, C. S. Yoo, J. Lang, D. Haskel, and G. Srajer, Appl. Phys. Lett. **90**, 042505 (2007).
[7] C. S. Yoo, H. Cynn, P. Soderlind, and V. Iota, Phys. Rev. Lett. **84**, 4132 (2000).
[8] H. Fujihisa and K. Takemura, Phys. Rev. B **54**, 5 (1996).
[9] F. Frey, W. Prandl, J. Schneider, C. Zeyen, and K. Ziebeck, J. Phys. F: Met. Phys. **9**, 603 (1979).
[10] P. Tolédano, G. Krexner, M. Prem, H. P. Weber, and V. P. Dmitriev, Phys. Rev. B **64**, 144104 (2001).
[11] R. V. Colvin and S. Arajs, J. Phys. Chem. Solids **26**, 435 (1965).
[12] L. Crovini, R. E. Bedford, and A. Moser, Metrologia **13**, 197 (1977).
[13] A. F. Goncharov, J. Crowhurst, and J. M. Zaug, Phys. Rev. Lett. **92**, 115502 (2004).
[14] P. Lazor, *Faculty of Science and Technology* (University of Uppsala, Uppsala, 1994).
[15] C. S. Yoo, P. Soderlind, and H. Cynn, J. Phys.: Condens. Matter **10**, L311 (1998).
[16] G. Steinle–Neumann, L. Stixrude, and R. E. Cohen, Phys. Rev. B **60**, 791 (1999).
[17] P. Modak, A. K. Verma, R. S. Rao, B. K. Godwal, and R. Jeanloz, Phys. Rev. B **74**, 012103 (2006).
[18] H. Olijnyk and A. P. Jephcoat, Solid State Commun. **115**, 335 (2000).
[19] J. C. Upadhyaya, D. K. Sharma, D. Prakash, and S. C. Upadhyaya, Can. J. Phys. **72**, 61 (1994).
[20] D. Antonangeli, M. Krisch, G. Fiquet, J. Badro, D. L. Farber, A. Bossak, and S. Merkel, Phys. Rev. B **72**, 134303 (2005).
[21] D. Antonangeli, M. Krisch, G. Fiquet, D. L. Farber, C. M. Aracne, J. Badro, F. Occelli, and H. Requardt, Phys. Rev. Lett. **93**, 215505 (2004).
[22] J. C. Crowhurst, D. Antonangeli, J. M. Brown, A. F. Goncharov, D. L. Farber, and C. M. Aracne, Appl. Phys. Lett. **89**, 111920 (2006).
[23] D. Antonangeli, S. Merkel, and D. L. Farber, Geophys. Res. Lett. **33**, L24303 (2006).
[24] D. J. Singh, *Planewaves, Pseudopotentials and the LAPW Method* (Kluwer, Norwell, 1994).
[25] J. P. Perdew, K. Burke, and M. Ernzerhof, Phys. Rev. Lett. **77**, 3865 (1996).
[26] L. Stixrude, R. E. Cohen, and D. J. Singh, Phys. Rev. B **50**, 6442 (1994).
[27] M. Körling and J. Häglund, Phys. Rev. B **45**, 13293 (1992).
[28] H. J. Monkhorst and J. D. Pack, Phys. Rev. B **13**, 5188 (1976).
[29] F. Birch, J. Geophys. Res. **83**, 1257 (1978).
[30] R. E. Cohen, L. Stixrude, and E. Wasserman, Phys. Rev. B **56**, 8575 (1997).
[31] G. Steinle–Neumann and R. E. Cohen, J. Phys.: Condens. Matter **16**, 8783 (2004).
[32] R. Hill, Proc. Phys. Soc., London, Sect. A **65**, 349 (1952).
[33] D. Antonangeli, L. R. Benedetti, D. L. Farber, G. Steinle-Neumann, A-L. Auzende, J. Badro, M. Hanfland, and M. Krisch, Appl. Phys. Lett. (to be published).
[34] H. R. Schober and H. Dederichs, *Elastic, Piezoelectric, Pyroelectric, Piezooptic, Electrooptic Constants and Nonlinear Dielectric Susceptibilities of Crystals*, Landolt-Börnstein, New Series, Group III, Vol. 11, Pt. A (Springer, New York, 1979), p. 40.
[35] H. J. McSkimin, J. Appl. Phys. **26**, 406 (1955).
[36] G. Simmons and H. Wang, *Single Crystal Elastic Constants and Calculated Aggregate Properties* (MIT, Cambridge, MA, 1971).
[37] T. S. Duffy, G. Shen, D. L. Heinz, J. Shu, Y. Ma, H. K. Mao, R. J. Hemley, and A. K. Singh, Phys. Rev. B **60**, 15063 (1999).
[38] F. Birch, Geophys. J. R. Astron. Soc. **4**, 295 (1961).
[39] B. Strauss, F. Frey, W. Petry, J. Trampenau, K. Nicolaus, S. M. Shapiro, and J. Bossy, Phys. Rev. B **54**, 6035 (1996).